Desalination and Water Treatment
www.deswater.com

doi: 10.5004/dwt.2018.21881

103 (2018) 40–48
January

Graphitic-like carbon nitride improved thermal stability and photocatalytic antifouling performance of polyether sulfone membranes

Manying Zhang[a,b,*], Minglai Fu[b], Kaisong Zhang[b,*]

[a]*School of Chemical and Environmental Engineering, Jiangsu University of Technology, Changzhou 213001, China, Tel. +86 592 6190782, Fax +86 592 6190534, email: myzhang@jsut.edu.cn (M.Y. Zhang)*
[b]*Institute of Urban Environment, Chinese Academy of Sciences, 1799, Jimei Road, Xiamen, China, Tel. +86 592 6190782, Fax +86 592 6190534, email: kszhang@iue.ac.cn (K.S. Zhang)*

Received 5 June 2017; Accepted 28 December 2017

ABSTRACT

The poor thermal tolerance of organic membrane and membrane fouling are two of the main obstacles for wider application of membrane process. Adding inorganic compounds which own fascinating chemical property and thermal stability as the additives may be an effective method to alleviate the problems. In this study, different amount of graphitic carbon nitride (g-C_3N_4) were introduced into polyether sulfone (PES) membranes by the phase-inversion method. The impacts of the g-C_3N_4 addition on the structure, thermal stability, filtration property and photocatalysis of g-C_3N_4/PES nano composite membranes were systematically studied. The results illustrated that the g-C_3N_4 well dispersed into PES matrix without obvious aggregation. The g-C_3N_4 introduction slightly improved the hydrophilicity of the nano composite membrane and did not sacrifice the separation property. The thermal stability of g-C_3N_4/PES nano composite membranes was examined in terms of thermogravimetric analyses (TGA) and water flux recovery ratio (FRR) after which were heated treatment at different temperature (50–80 °C) for different times (30–240 s). The results revealed that the thermal stability and the filtration performance of PES membrane were significantly improved by the incorporation of g-C_3N_4 nanosheets. Also the addition of g-C_3N_4 nanosheets could endow the nanocomposite membranes with photocatalytic antifouling property.

Keywords: Graphitic carbon nitride; Thermal stability; Photocatalysis; Antifouling

1. Introduction

Membrane filtration is an efficient way to remove particulates or dissolved matters in waste water treatment. Due to the reliability and ease of operation, membrane filtration systems have been widely used in many fields. Polymers such as polyethersulfone (PES) [1,2], polysulfone (PS) [3], polyvinylidene fluoride (PVDF) [4,5], cellulose acetate (CA) [6] and polyamide [7] are all attractive membrane materials because of their outstanding solubility, thermoplastic process ability and mechanical characteristics. However, membrane technology still faces many problems during its wider application now.

For example, the poor thermal tolerance of organic membrane is one of the key disadvantages compared with inorganic membrane and has attracted much attention in both organic membrane fabrication and application processes [8,9]. The application of high-temperature membranes is increasingly needed in food or medical industry because of the production of a large number of high temperature sterilization liquid. The increased demands for the thermal stability membranes have attracted much more attentions [10].

Moreover, membrane fouling is considered to be another main obstacle which results in the significant decline in filtration performance, the increased maintenance costs and shortened membrane life [1]. Therefore, many efforts

*Corresponding author.

1944-3994 / 1944-3986 © 2018 Desalination Publications. All rights reserved.

have been taken to improve the overall performances of membrane.

Many papers reported that inorganic nanomaterials were introduced into polymeric matrix to endow the nanocomposite membranes with desired properties. Some efforts have been made to improve the thermal stability of materials. Dong et al. [11] reported even the introduction of 0.5 wt% melanins could promote the thermal stability of poly (vinyl alcohol) (PVA). Graphene, as a two-dimensional (2D) carbon material, has become the hot spot research because of the excellent thermal, electrical and mechanical properties [12]. Many papers have reported that the combination of graphene with polymers significantly enhanced the thermal stability of nanocomposites. Bao et al. [13] found that the addition of 1.6 wt% graphene could improve the thermal stability of PVA nanocomposites. Guo et al. [14] reported the improved thermal stability of graphene/PVA nanocomposite with only 0.2 wt% addition of graphene. As mentioned in previous papers [15,16], the formation of stable hydrogen bonding induced the increased thermal stability of PVA nanocomposites.

Nano titanium dioxide (TiO_2) as a traditional photocatalyst has been widely incorporated into various polymeric materials [1]. Many reports showed the significanltly enhanced surface hydrophilicity, improved photocatalytic and antifouling performances with the introduction of TiO_2 [4–6]. In addition to these merits, the TiO_2 based nanocomposite membrane still faces the challenge of poor photocatalytic performance under visible light irradiation [6]. Thus, using a new nanomaterial to address above problems has become an urgent need.

Graphitic carbon nitride (g-C_3N_4), which has similar stacked 2D layered structure to graphene, exhibits excellent visible light photocatalysis, chemical and thermal stability, and has attracted increasing research attention [17–19]. Shi et al. [17] reported the addition of different loading levels of g-C_3N_4 into sodium alginate (SA) could obviously increase the thermal stability with the increased initial and half thermal degradation temperature. Recently, Zhao et al. [6] successfully introduced g-C_3N_4 on the surface of CA membrane by vacuum filtration. They found that the addition of g-C_3N_4 could enhance the degradation ability of organic pollutants. However, membrane surface modification may raise problems during long time filtration such as the release of particles because of the poor adhesion between photocatalyst and membrane substrate. Alternatively, blending modification is an attractive method due to its facile preparation and stable performance [6].

So far, no study on investigation into the comprehensive impacts of g-C_3N_4 incorporation with membrane matrix by blending on the thermal stability, filtration, photo catalytic and anti fouling performances of ultra filtration (UF) process has been reported. Hence, considering the similar structure of g-C_3N_4 and graphene, by introducing g-C_3N_4 into membrane matrix by simply blending to fabricate hybrid membranes, it is expected that the addition of g-C_3N_4 could not only effectively enhance the thermal stability but also the photo catalytic and anti fouling performances of the membrane.

Thus, the paper was from a different perspective to study the comprehensive impacts of g-C_3N_4 on the performances of g-C_3N_4/PES nanocomposite membranes. In this work, the effect of g-C_3N_4 nanosheet on filtration property at increased temperatures was studied. The influence of inorganic additive on the stabilization of polyethersulfone (PES) membranes upon heating treatment was examined by the calculation of water flux recovery ratio (FRR) and TGA test. Also the photo catalytic performance and fouling mitigation capacity of nanocomposite membranes were tested by the dye degradation experiment and bovine serum albumin (BSA) filtration under visible light illumination.

2. Experimental

2.1. Materials

PES (Ultrason E6020P) was purchased from BASF. Melamine (Analytical grade), sulfuric acid (H_2SO_4, analytical grade), nitric acid (HNO_3, analytical grade), N, N-dimethyl for mamide (DMF), methyl orange (MO), Bovine serum albumin (BSA, 69 kDa), egg albumin (45 kDa), pepsin (35 kDa) were purchased from Sigma Aldrich.

2.2. Preparation and characterization of g-C_3N_4

In a typical synthesis, 5 g of melamine was heated at 500°C in a muffle furnace for 2 h and following elevated to the 520°C with a step of 10°C min^{-1} for another 2 h for the further reaction. The resultant yellow powder were first dispersed in the mixture of nitric acid and sulfuric acid with the volume ratio of 3:1, then the turbid liquid was magnetic stirred overnight, the resultant powder was washed by deionized water completely until the neutral and following baked in the oven overnight to get the modified g-C_3N_4 samples.

The morphology of g-C_3N_4 was characterized by transmission electron microscopy (TEM, Tecnai F30). The crystal structure of g-C_3N_4 was examined by X-ray diffraction (XRD, X' Pert PRO) at a scanning rate of 10°min^{-1} in the range of 10–80°. The chemical structure of g-C_3N_4 was studied by Fourier transform infrared spectrometer (FTIR) (Thermo Fisher Scientific).

2.3. Membranes fabrication

Different contents of dry g-C_3N_4 powder were added into DMF and well dispersed by ultrasonic. Then PES was dissolved and heated at 60°C until completely dissolved. The solution was degassed at 60°C and then scattered on the nonwoven fabric. The nascent membrane was dipped in pure water (25 ± 1°C) to induce phase inversion. The dope solution was prepared as shown in Table 1.

2.4. Characterization

The morphologies of the membranes were observed by scanning electron microscopy SEM (Hitachi S-4800) after coating with gold.

The hydrophilicity of the membrane was evaluated by testing the contact angle with the instrument (CAM200, KSV). In order to minimize the error, the measurements were conducted at six different locations to get the average value.

Table 1
The basic parameters of various membranes

Membrane abbreviation	C_3N_4 content (%)	PES (%)	DMF (%)	MWCO (KDa)	CA (°)
M0	0	18	82	45	68.5 ± 3.6
M1	0.25	18	81.75	45	63.2 ± 3.1
M2	0.50	18	81.50	45	60.4 ± 3.7
M3	0.75	18	81.25	45	62.9 ± 2.8
M4	1.00	18	81.00	45	61.4 ± 1.4

To evaluate the thermal stability of g-C_3N_4/PES nanocomposite membrane, thermogravimetric analyses (TGA, Perkin Elmer) were performed between 40–800°C at the heating rate of 10°C min^{-1} under nitrogen atmosphere.

2.5. Permeate flux measurements

UF experiment was conducted in a dead-end stirred cell at 0.1 MPa [1,4,5]. The water flux (J) was calculated with Eq. (1)

$$J = \frac{V}{A\Delta t} \tag{1}$$

where V (L) is the volume of permeated water, A (m^2) is the membrane area and Δt (h) is the filtration time.

Molecular weight cut-off (MWCO) is a parameter that reflects the pore size of membrane. It can be obtained by the protein rejection (R) calculation of different molecular weight such as BSA (69 kDa), egg albumin (45 kDa), pepsin (35 kDa) and trypsin (24 kDa) with Eq. (2).

$$R = \left(1 - \frac{C_p}{C_f}\right) \times 100\% \tag{2}$$

where C_p and C_f (g L^{-1}) are the permeate and feed proteins concentrations. The rejection tests were conducted at 25°C with a feed pressure of 0.1 MPa.

2.6. The characterization of membrane thermal stability

The effect of g-C_3N_4 incorporation on the thermal stability of nanocomposite membranes was reflected by the pure water flux test. First, the pure water permeate (J_{w1}) and the trypsin rejection were measured. Then the samples were heated treatment at different temperature (50–80°C) for different times (30–240 s). Finally, the water permeate (J_{w2}) and the protein rejection were tested again. The flux recovery ratio (FRR) after heating can be got as:

$$FRR = \left(\frac{J_{w2}}{J_{w1}}\right) \times 100\% \tag{3}$$

2.7. Photocatalytic property of membranes

Photocatalytic performance was firstly tested by degradation of methyl orange (MO) imprint on membrane surface [6]. 100 μL of MO (10 mg L^{-1}) was dripped on the membrane surface to form a yellow imprint. Then all the membranes were exposed to the xenon lamp with a 420 nm cut off filter irradiation for 3 min. The pure PES membrane was tested under the same condition.

Then the photocatalysic property of various membranes were further tested by the degradation of MO solution under the visible-light irradiation. First, the membrane was anchored to the bottom of the petri dish using double-sided tape to form a flat membrane surface. Then 50 mL of MO solution (10 mg L^{-1}) was filled in to ensure the fully contact between membrane and dye molecules. 3 mL solution was collected every 20 min to test the absorption value at 505 nm.

2.8. The antifouling characteristics in photocatalysis

In order to compare the anti fouling performance of various membranes, the filtration experiments included four steps were conducted as follows. Firstly, the pure water flux (J_{w1}) was recorded for 0.5 h. Then the BSA solution (1 g L^{-1}) was fed in the cell and the flux (J_p) was recorded. The fouled membranes were cleaned by deionized water and the third flux (J_{rw}) was measured. Finally, in order to prove the photo catalysis anti fouing property of nanocomposite membrane, the BSA fouled membrane was irradiated by the xenon lamp for 1 h and the flux (J_{w2}) were recorded again in order to get the flux recovery ratio. The FRR before and after visible light irradiation can be got using Eq. (3).

Moreover, the fouling resistance parameters were analyzed to study the fouling process. The irreversible (Rir), reversible (Rr) and total fouling ratio (R_t) were calculated as [1,5]:

$$R_t = \left(1 - \frac{J_p}{J_{w1}}\right) \times 100 \tag{4}$$

$$R_r = \left(\frac{J_{w2} - J_p}{J_{w1}}\right) \times 100 \tag{5}$$

$$R_{ir} = \left(\frac{J_{w1} - J_{w2}}{J_{w1}}\right) \times 100 \tag{6}$$

3. Results and discussion

3.1. The characterization of g-C_3N_4

TEM was used to observe the morphology of g-C_3N_4. The g-C_3N_4 exhibits a typical rippled 2D paper-like structure (Fig. 1), which is in agreement with the previous reports [17,19].

The XRD pattern of g-C_3N_4 is shown in Fig. 2. Two characteristic peaks at 12.8°and 27.1° which corresponds to the (100) and (002) diffraction planes are attributed to the in-plane structure packing of tristriazine units and interlayer-stacking reflection respectively [19–22].

The chemical structure of g-C_3N_4 was further characterized by FTIR analysis. Fig. 3 shows the typical molecular structure of g-C_3N_4. The broad peak at 3000–3500 cm^{-1} is ascribed to the N-H stretching vibration and surface adsorbed water molecules [19,23]. The peak at 808 cm^{-1} may

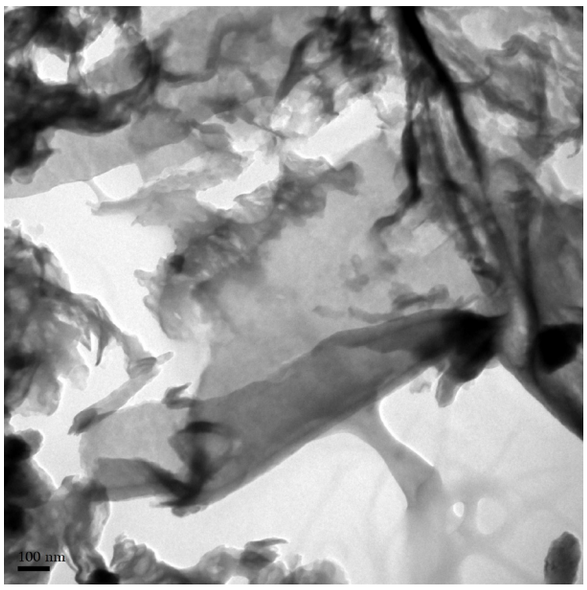

Fig. 1. TEM morphology of g-C_3N_4 nanosheet.

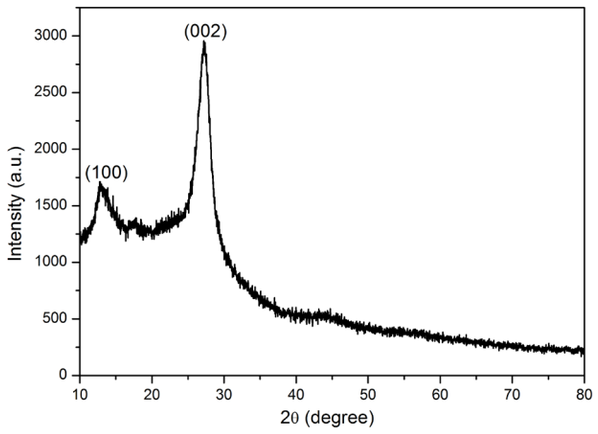

Fig. 2. XRD pattern of the g-C_3N_4 nanosheet.

be assigned to the breathing of triazine units [17,21,24]. The multiple peaks in the 1200–1700 cm^{-1} region, with the characteristic peaks at and 1240 and 1652 cm^{-1}, may be assigned to the stretching vibration of CN heterocycles [6,21,24].

3.2. Characterization of g-C_3N_4/PES membranes

3.2.1. Membrane morphology

As shown in Fig. 4a, various membranes all have smooth and clean surfaces. No significant nanomaterials aggregation was observed, indicating that the addition of g-C_3N_4 has none or little effects on the membrane surface structure.

Fig. 4b shows the prepared membranes own a dense selective layer, a thicker finger-like layer and macro pores at the bottom which is the typical asymmetric structure. Compared to M0, the finger-like voids in modified membrane

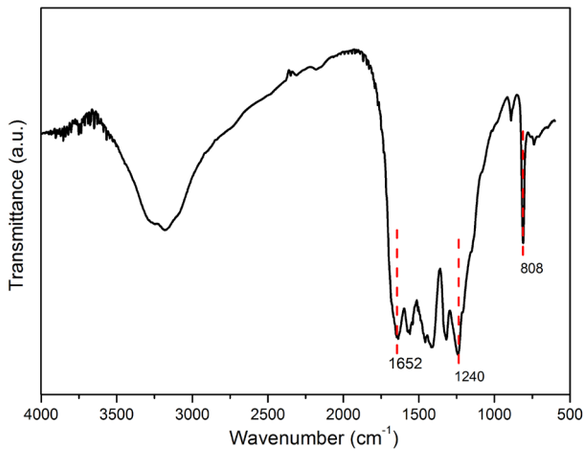

Fig. 3. The FTIR characterization of g-C_3N_4 nanosheet.

with g-C_3N_4 loading of 0.5% (M2) become wider and elongate across the whole cross section, which may improve the membrane flux. However, the effect didn't maintain when the concentration of g-C_3N_4 was up to 1.0%. It is considered that the relative diffusion rate and driving force have great influences on membrane structure [25]. The presence of g-C_3N_4 nanosheets may enhance the instability of casting solution and induce the accelerated demixing process. The accelerated demixing process may facilitate the fully development of the finger-like micro voids in M2 [26]. As for M4, the more addition of g-C_3N_4 could increase the viscosity of casting solutions which decreased the diffusion of non-solvent. Thus the growth of macrovoids can be inhibited [27, 28].

3.2.2. Hydrophilicity and pore size of nanocomposite membranes

The contact angles were used to evaluate the surface hydrophilicity as shown in Table 1. The contact angle of M0 was 68.5°, which was consistent with previous results [29, 30]. The overall contact angle slightly decreased with the incorporation of g-C_3N_4, which indicated the hydrophilicity of membrane was increased by g-C_3N_4. The existence of hydrophilic groups such as $–NH_2$ or –NH after treated by sulfuric acid and nitric acid may be responsible for the hydrophilicity increase [31]. This is also confirmed by FTIR results as shown in Fig. 3.

Molecular weight cut-off (MWCO) is an important parameter to reflect the UF membrane pore size. As shown in Table 1, all the membranes have the same MWCO of 45 KDa indicating that the additions of g-C_3N_4 nanosheets do not significantly change the membrane pore size.

3.3. The study of thermal stability of nanocomposite membranes

3.3.1. TGA tests

The TGA test was conducted to compare the thermal properties of samples as shown in Fig. 5. All the sam-

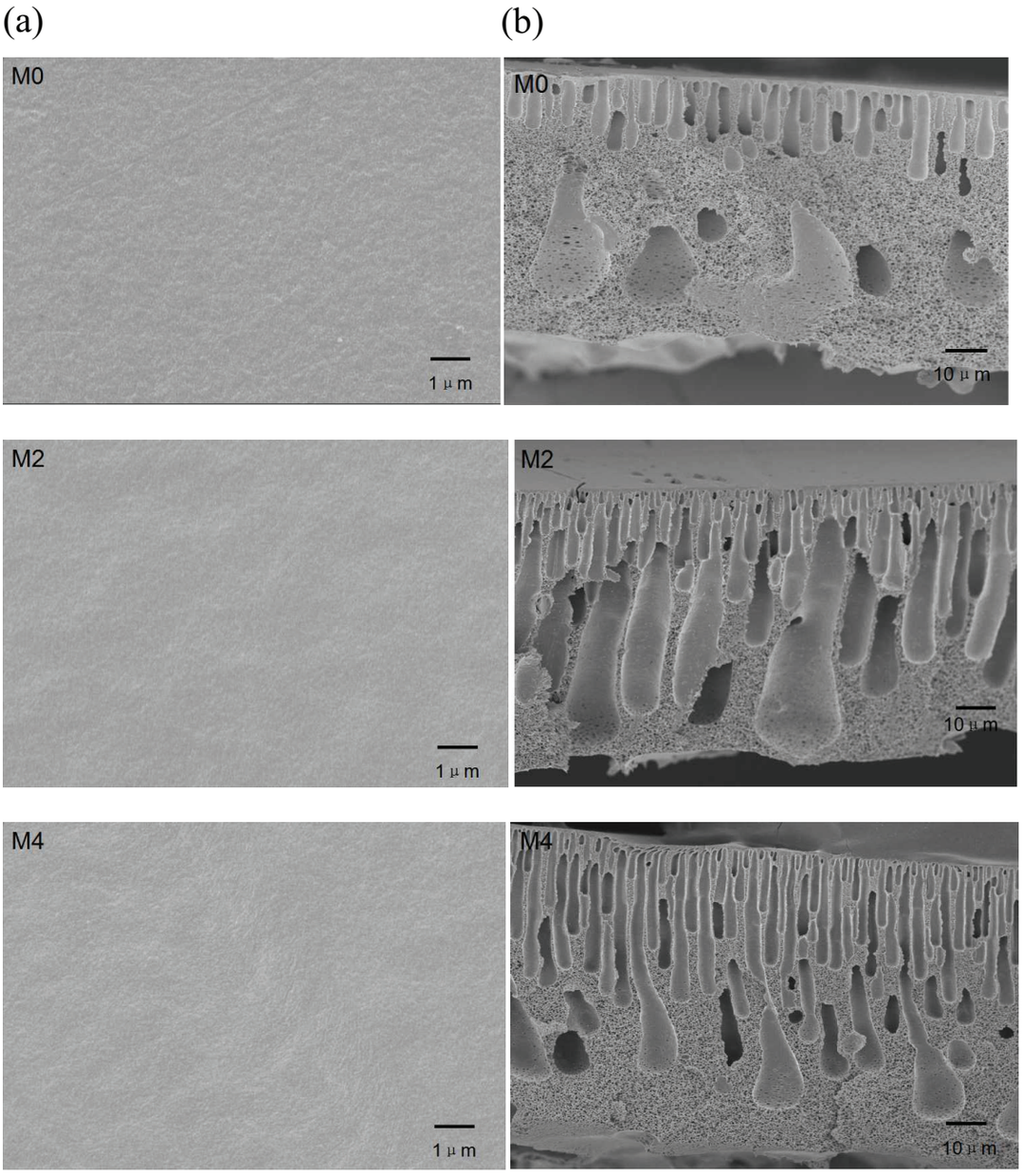

Fig. 4. The SEM morphologies of membranes. (a) surface, (b) cross section.

ples exhibited single-step decomposition which indicated the good compatibility of g-C_3N_4 and polymer. The small mass loss below 400°C may be assigned to the volatilization of adsorbed water or the residual solvent in the membranes. The decomposition of polymer may be responsible for the significant mass decrease between 400–750°C. The little shift of TGA curves indicates the addition of g-C_3N_4 nanosheets can increase the degradation temperature and enhanced the thermal stability of membranes [17,32,33]. This may attribute to the fact that more heat was absorbed by the g-C_3N_4 nanosheets in the membranes during heating-up, also the fillers improved mass transport barrier effect during decomposition [17,32,34].

3.3.2. The filtration property and flux recovery ratio tests

Dead-end filtration were performed to study the pure water flux of all the samples as shown in Fig. 6. The water flux of all the nanocomposite membranes was higher than PES membranes and M2 had the highest flux of 339 L m^{-2} h^{-1}. Considering all the membranes have the same MWCO, the changes in flux with the incorporation of g-C_3N_4 may be clarified as below. Firstly, the incorporation of g-C_3N_4 improved

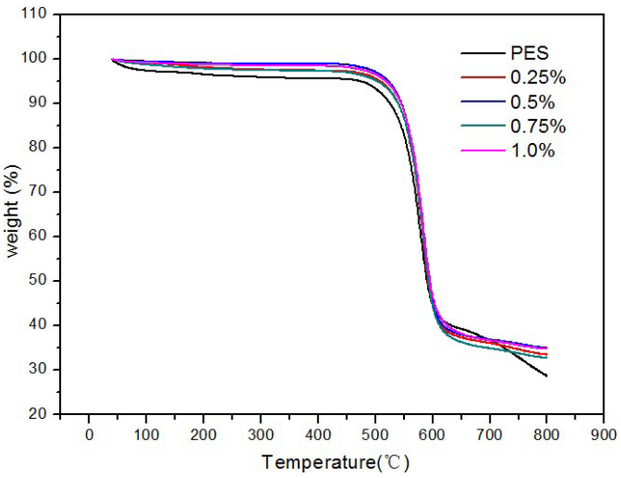

Fig. 5. TGA curves for the g-C_3N_4/PES composite membranes.

the hydrophilicity of the nanocomposite membranes which may further improve the water uptake property. Secondly, the introduction of g-C_3N_4 enlarged the finger-like pore and improved the inter-connectivity of cross section pore structure, which reduced the hydraulic resistance and enhanced the flux permeate. However, the water flux slightly reduced when further improved the g-C_3N_4 content to 1.0%, which might be explained by the corresponding cross section morphology changes as shown in Fig. 4 and the contact angle changes in Table 1.

The flux recovery ratio (FRR) was used to indicate the effect of heating on the membrane filtration property. Fig. 6 shows the flux recovery ratio (FRR, %) of all the membranes after heated at 60°C for 2 min. As shown in Fig. 6, the flux of all the samples decreased and the impact was much less for the g-C_3N_4/PES composite membranes. As for the pure PES membrane (M0), the flux declined to 19.5% of its initial flux. The flux recovery ratio (FRR, %) remained at 81.5%, 85.8%, 77.8% and 68.8% for the g-C_3N_4 modified membranes respectively, which was much higher than M0.

The trypsin rejection of all the membranes was relatively low and around 18% as shown in Fig. 7. This is because that the molecular weight of trypsin (24 KDa) is much smaller than the MWCO of 45 KDa. After heat treatment, the trypsin rejection of all the membranes increased significantly which is consistent with the pure water flux changes. The results indicated that heat treatment probably brings about the shrinkage of the pore structure and the decrease of surface porosity. This negative change is more significant for pure PES membrane, showing that g-C_3N_4 as an effctive addtive could maintain the stability of the membrane structure to some extent.

As the M2 sample showed the best filtration performance in Fig. 6, much detailed testes were conducted between M2 and M0 samples to compare the effect of g-C_3N_4 incorporation on the thermal stability of membranes. The samples were heated at 60°C for different times (30 s–240 s) as shown in Fig. 8. At the initial 90 s, the FRR was 72.2% and 80.3% for M0 and M2 respectively, which were relatively high. When the heating time was extended to 120 s, the water flux of M0 significantly declined as low as 19.5%. While as for the M2, the

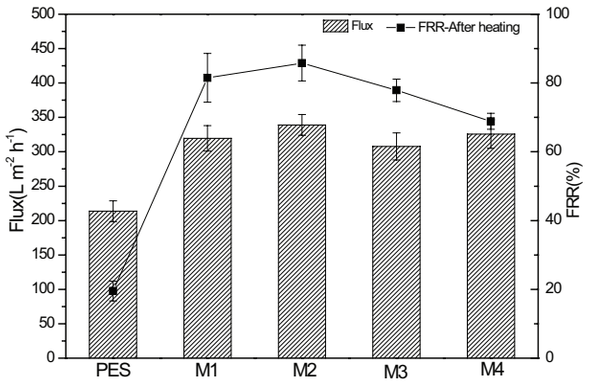

Fig. 6. The pure water flux and flux recovery ratio (FRR, %) of all the membranes after heated at 60°C for 2 min.

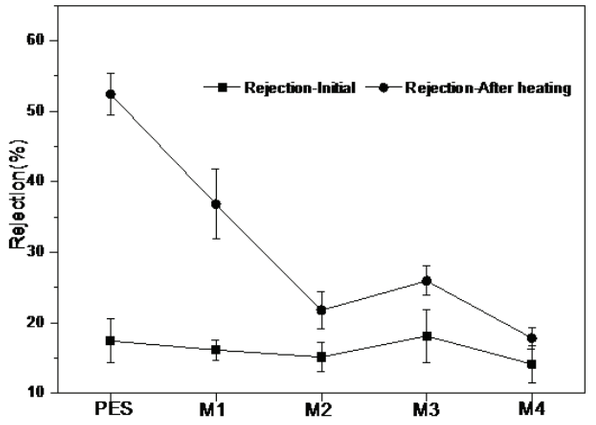

Fig. 7. The protein rejection properties of g-C_3N_4/PES composite membranes before and after heated treatment.

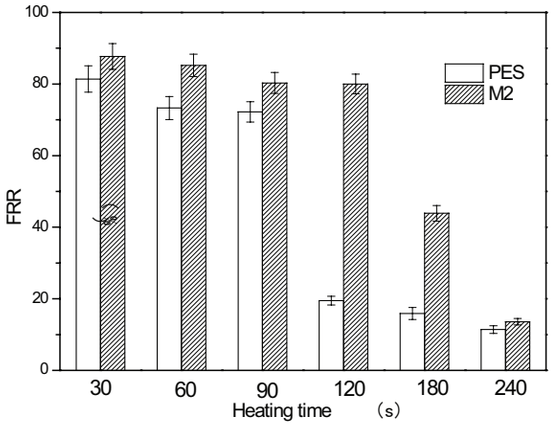

Fig. 8. The FRR of membranes after heated at 60°C for different times (30 s–240 s).

FRR still maintained as high as 80%. When the heating time was much longer, all the membranes showed very low FRR. It is clear that the introduction of g-C_3N_4 can effectively enhance the thermal stability of PES membrane during a certain time.

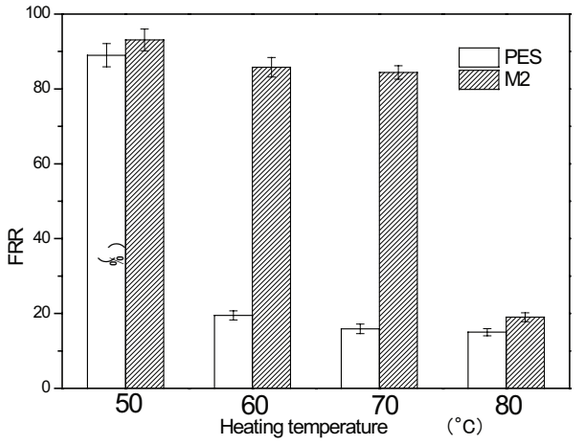

Fig. 9. The FRR of all the membranes after heated for 2 min at different temperature.

In addition, we studied the influence of 0.5% g-C_3N_4 incorporation on the filtration properties of PES membrane after heated at 50–80°C for 2 min. From Fig. 9 we can see that when the temperature was at 60°C or higher, the water flux of pure PES membrane decreased significantly to less than 20% of initial flux. While as for M2, the FRR was relatively much higher than M0 when the temperature was below 70°C. The situation disappeared when the temperature was at 80°C or higher.

Generally, the water flux was mainly influenced by the pore size, porosity and pore structure of membrane. The heat treatment may cause the pore structure collapsing thus significantly destroy the filtration performance of porous membranes. The results above clearly indicated that the incorporation of g-C_3N_4 may effectively restrain pore collapse upon drying within certain time and temperature.

3.4. Photocatalytic property of membranes

Methyl orange (MO) is a widely used organic dye. As reference, the visible-light photo degradation property of pure PES membrane was also investigated under the same condition. The short-term photo catalytic effect of various membranes was recorded by the camera. As shown in Fig. 10, the yellow imprint that formed by MO on pure PES membrane (M0) surface was still very clear and obvious under visible-light irradiation for 3 min. When the content of g-C_3N_4 was up to 1.0% (M4), the yellow imprint significantly became lighter. This suggested that the incorporation of g-C_3N_4 could endow the nanocomposite membrane with photo catalytic property. The similar phenomenon was also reported by Zhao et al. [6].

To further evaluate the relationship between photo catalytic property of nanocomposite membrane and the content of g-C_3N_4, the long-term degradation of MO was conducted. As shown in Fig. 11, almost no photo degradation effect of MO was observed for M0. This indicated that PES and nonwoven fabric didn't show any photocatalytic performance. In contrast, the introduction of

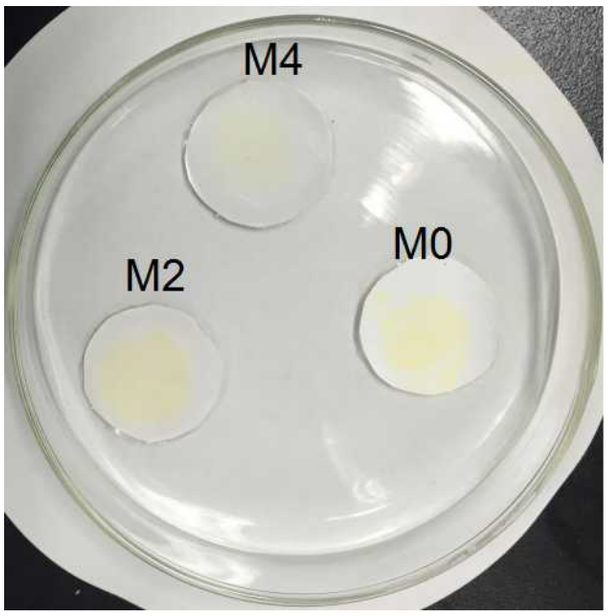

Fig. 10. The color change of MO imprint after irradiated under visible light for 3 min.

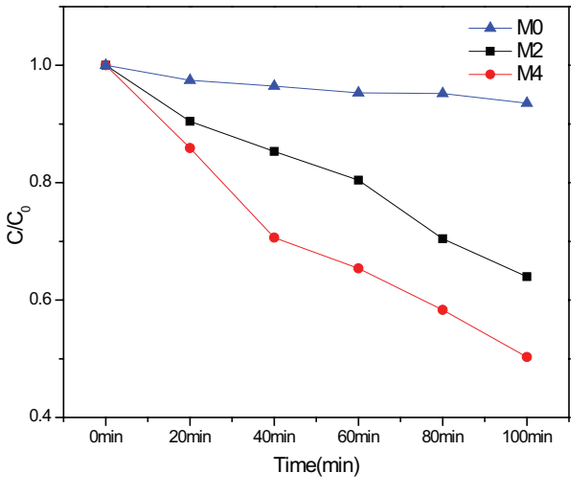

Fig. 11. Degradation rate of MO under visible light irradiation for various membranes.

g-C_3N_4 could enhance the photo catalytic activity of nanocomposite membranes under visible-light. The M2 owned 37% degradation efficiency toward MO. While the degradation activity improved a lot with the increase of g-C_3N_4 content. As for M4, the degradation efficiency was up to 50%. The results above confirmed that the incorporation of g-C_3N_4 could significantly increase the photo catalytic activity of nanocomposite membrane under visible-light irradiation.

The possible degradation mechanism under visible-light was mainly attributed to the generation of photo-elec-

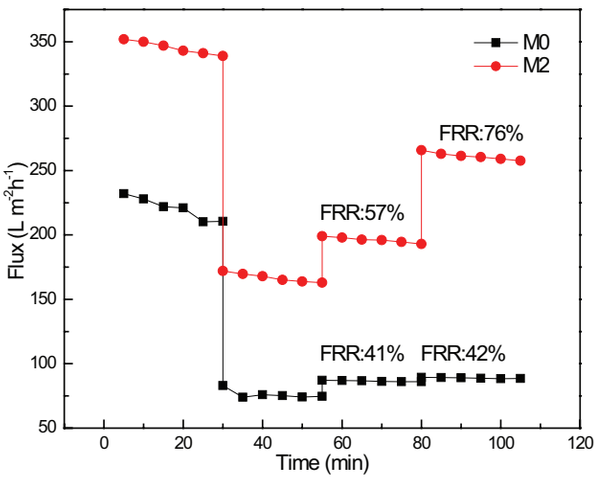

Fig. 12. Time-dependent flux of membranes and the flux recovery ratio before and after xenon lamp illumination.

trons (e^-) and holes (h^+) by g-C_3N_4. The oxygen molecule (O_2) can capture the electrons to produce O_2^-, HO_2^-, H_2O_2 and •OH. The holes can also interact with water molecule and hydroxyl group (OH^-) to produce •OH. The •OH can degrade many kinds of complex organic materials [4–6].

3.5. The antifouling performance of membranes in photo catalysis

To study the alleviative effect of photo catalysis on membrane fouling, the BSA filtration tests were conducted. As shown in Fig. 12, the water flux declined sharply during BSA filtration step, which is attributed to the deposition of BSA and the formation of cake layers on membrane surfaces. After simple water rinsing, the flux of M0 recovered 41%, and the g-C_3N_4 modified membrane (M2) recovered 57%. This indicated that the loosely bound BSA and the cake layer can be removed by hydraulic shear force. After the supply of visible light illumination following water rinsing, further flux increase was observed for M2 and the flux recovery ratio reached to 76%. But as for M0, no significant flux increment was observed.

To further investigate the membrane fouling details, the different fouling resistances were calculated as shown in Fig. 13. The g-C_3N_4 modified membrane (M2) had a obvious lower R_t than M0. The initial R_r values after water rinsing of M0 and M2 were 5.4% and 8.8% respectively. After the visible light illumination, the R_r value of M2 significantly increased to 27.9%. While the R_r of M0 was still as low as 6.5%. The results in Figs. 12 and 13 are consistent with each other, indicating the improved antifouling performance of membranes with the addition of g-C_3N_4.

As mentioned above, the •OH that generated by g-C_3N_4 under visible light irradiation can degrade many kinds of complex organic materials [4–6]. The filtration results confirmed that the •OH can induce the degradation of strongly bound pollutants and make the pollutants more easier to be removed from membrane surface, thus improving the anti fouling property of nanocomposite membranes.

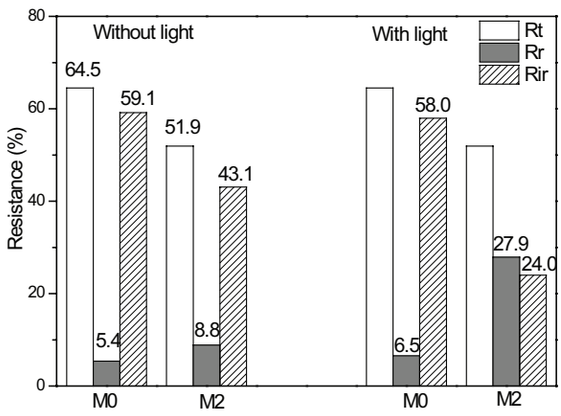

Fig. 13. Fouling resistance of membranes before and after visible light illumination.

4. Conclusions

In this study, a novel g-C_3N_4/PES ultra filtration membrane was successfully fabricated by phase-inversion method. The incorporation of g-C_3N_4 into PES membranes as additives was systematically studied. The SEM pictures illustrated that the g-C_3N_4 were well distributed in the membrane and no visual aggregation was observed. The membrane hydrophilicity was slightly enhanced due to the introduction of g-C_3N_4 nanosheets. The TGA test and filtration performance results revealed significantly improvement of thermal stability of the modified membranes. The dye degradation experiments under visible light irradiation confirmed the significantly improved photo catalytic activity of nano composite membrane by the incorporation of g-C_3N_4 nanosheets. The BSA filtration experiments indicated the introduction of g-C_3N_4 can endow PES membrane with self-cleaning property and improve the anti fouling performance. The work may contribute to a potential research of the g-C_3N_4 in advanced membrane materials. All advantages shown by the g-C_3N_4/PES nanocomposite membrane make it promising for wider industrial application.

Acknowledgments

This work was supported by the National Natural Science Foundation of China (51508239) and Jiangsu province (BK20150245, BY2016030-01) and Qing Lan Project, Bureau of International Cooperation, CAS.

References

[1] M. Safarpour, V. Vatanpour, A. Khataee, Preparation and characterization of graphene oxide/TiO_2 blended PES nanofiltration membrane with improved anti fouling and separation performance, Desalination, 393 (2016) 65–78.

[2] A. Ananth, G. Arthanareeswaran, A.F. Ismail, Y.S. Mok, T. Matsuura, Effect of bio-mediated route synthesized silver nanoparticles for modification of polyether sulfone membranes, Colloids Surf. Physicochem. Eng. Aspects, 451 (2014) 151–160.

[3] D.Y. Koseoglu-Imer, B. Kose, M. Altinbas, I. Koyuncu, The production of polysulfone (PS) membrane with silver nanoparticles (AgNP): Physical properties, filtration performances, and biofouling resistances of membranes, J. Membr. Sci., 428 (2013) 620–628.
[4] Y. Zhang, M. Cui, Porous YxFeyZr1–x–yO_2 coated TiO_2 solid superacid particles/PVDF hybrid membranes with anti-fouling property, Chem. Eng. J., 301 (2016) 342–352.
[5] Y. Zhang, L. Wang, Y. Xu, ZrO_2 solid super acid porous shell/void/TiO_2 core particles (ZVT)/polyvinylidene fluoride (PVDF) composite membranes with anti-fouling performance for sewage treatment, Chem. Eng. J., 260 (2015) 258–268.
[6] H. Zhao, S. Chen, X. Quan, H. Yu, H. Zhao, Integration of micro filtration and visible-light-driven photo catalysis on g-C_3N_4 nanosheet/reduced graphene oxide membrane for enhanced water treatment, Applied Catalysis B: Environmental, 194 (2016) 134–140.
[7] J. Yin, Y. Yang, Z. Hu, B. Deng, Attachment of silver nanoparticles (AgNPs) onto thin-film composite (TFC) membranes through covalent bonding to reduce membrane biofouling, J. Membr. Sci., 441 (2013) 73–82.
[8] M.N. Abu Seman, M. Khayet, N. Hilal, Development of antifouling properties and performance of nanofiltration membranes modified by inter facial polymerisation, Desalination, 273 (2011) 36–47.
[9] T. Shintani, H. Matsuyama, N. Kurata, Effect of heat treatment on performance of chlorine-resistant polyamide reverse osmosis membranes, Desalination, 247 (2009) 370–377.
[10] Y. Dai, X. Jian, S. Zhang, M.D. Guiver, Thin film composite (TFC) membranes with improved thermal stability from sulfonated poly(phthalazinone ether sulfone ketone) (SPPESK), J. Membr. Sci., 207 (2002) 189–197.
[11] W. Dong, Y. Wang, C. Huang, S. Xiang, P. Ma, Z. Ni, M. Chen, Enhanced thermal stability of poly(vinyl alcohol) in presence of melanin, J. Therm. Anal. Calorim., 115 (2014) 1661–1668.
[12] S.-S. Dong, F. Wu, L. Chen, Y.-Z. Wang, S.-C. Chen, Preparation and characterization of Poly(vinyl alcohol)/graphene nanocomposite with enhanced thermal stability using PEtVIm-Br as stabilizer and compatibilizer, Polym. Degrad. Stab., 131 (2016) 42–52.
[13] C. Bao, Y. Guo, L. Song, Y. Hu, Poly(vinyl alcohol) nanocomposites based on graphene and graphite oxide: a comparative investigation of property and mechanism, J. Mater. Chem., 21 (2011) 13942–13950.
[14] J. Guo, L. Ren, R. Wang, C. Zhang, Y. Yang, T. Liu, Water dispersible graphene noncovalently functionalized with tryptophan and its poly(vinyl alcohol) nanocomposite, Composites Part B: Engineering, 42 (2011) 2130–2135.
[15] X. Yang, L. Li, S. Shang, X.-m. Tao, Synthesis and characterization of layer-aligned poly(vinyl alcohol)/graphene nanocomposites, Polymer, 51 (2010) 3431–3435.
[16] H.K.F. Cheng, N.G. Sahoo, Y.P. Tan, Y. Pan, H. Bao, L. Li, S.H. Chan, J. Zhao, Poly(vinyl alcohol) nanocomposites filled with poly(vinyl alcohol)-grafted graphene oxide, ACS Appl. Mater. Interfaces, 4 (2012) 2387–2394.
[17] Y. Shi, S. Jiang, K. Zhou, C. Bao, B. Yu, X. Qian, B. Wang, N. Hong, P. Wen, Z. Gui, Y. Hu, R.K.K. Yuen, Influence of g-C_3N_4 nanosheets on thermal stability and mechanical properties of biopolymer electrolyte nanocomposite films: a novel investigation, ACS Appl. Mater. Interfaces, 6 (2013) 429–437.
[18] X.J. Bai, R.L. Zong, C.X. Li, D. Liu, Y.F. Liu, Y.F. Zhu, Enhancement of visible photo catalytic activity via Ag@C_3N_4 core-shell plasmonic composite, Appl. Catal. B-Environ., 147 (2014) 82–91.
[19] W. Zhang, L. Zhou, H. Deng, Ag modified g-C_3N_4 composites with enhanced visible-light photo catalytic activity for diclofenac degradation, J. Mol. Catal. A: Chem., 423 (2016) 270–276.
[20] L.C. Chen, X.T. Zeng, P. Si, Y.M. Chen, Y.W. Chi, D.H. Kim, G.N. Chen, Gold nanoparticle-graphite-like C_3N_4 nanosheet nanohybrids used for electrochemiluminescent immunosensor, Anal. Chem., 86 (2014) 4188–4195.
[21] L. Liu, Y. Qi, J. Lu, S. Lin, W. An, Y. Liang, W. Cui, A stable Ag_3PO_4@g-C_3N_4 hybrid core@shell composite with enhanced visible light photo catalytic degradation, Appl. Catal. B: Environ., 183 (2016) 133–141.
[22] M.J. Muñoz-Batista, O. Fontelles-Carceller, M. Ferrer, M. Fernández-García, A. Kubacka, Disinfection capability of Ag/g-C_3N_4 composite photo catalysts under UV and visible light illumination, Appl. Catal. B: Environ., 183 (2016) 86–95.
[23] M. Faisal, A.A. Ismail, F.A. Harraz, S.A. Al-Sayari, A.M. El-Toni, M.S. Al-Assiri, Synthesis of highly dispersed silver doped g-C_3N_4 nanocomposites with enhanced visible-light photo catalytic activity, Mater. Design, 98 (2016) 223–230.
[24] S.C. Yan, Z.S. Li, Z.G. Zou, Photo degradation performance of g-C_3N_4 fabricated by directly heating melamine, Langmuir, 25 (2009) 10397–10401.
[25] W. Zhao, Y. Su, C. Li, Q. Shi, X. Ning, Z. Jiang, Fabrication of anti fouling polyether sulfone ultra filtration membranes using Pluronic F127 as both surface modifier and pore-forming agent, J. Membr. Sci., 318 (2008) 405–412.
[26] X. Li, X. Fang, R. Pang, J. Li, X. Sun, J. Shen, W. Han, L. Wang, Self-assembly of TiO_2 nanoparticles around the pores of PES ultra filtration membrane for mitigating organic fouling, J. Membr. Sci., 467 (2014) 226–235.
[27] S.A. McKelvey, W.J. Koros, Phase separation, vitrification, and the manifestation of macrovoids in polymeric asymmetric membranes, J. Membr. Sci., 112 (1996) 29–39.
[28] J. Huang, K.S. Zhang, K. Wang, Z.L. Xie, B. Ladewig, H.T. Wang, Fabrication of polyethersulfone-mesoporous silica nanocomposite ultra filtration membranes with anti fouling properties, J. Membr. Sci., 423 (2012) 362–370.
[29] V. Vatanpour, S.S. Madaeni, R. Moradian, S. Zinadini, B. Astinchap, Fabrication and characterization of novel anti fouling nano filtration membrane prepared from oxidized multiwalled carbon nanotube/polyethersulfone nanocomposite, J. Mater. Sci., 375 (2011) 284–294.
[30] M. Zhang, K. Zhang, B. De Gusseme, W. Verstraete, Biogenic silver nanoparticles (bio-Ag^0) decrease biofouling of bio-Ag^0/PES nanocomposite membranes, Water Res., 46 (2012) 2077–2087.
[31] M.J. Bojdys, J.-O. Müller, M. Antonietti, A. Thomas, Ionothermal synthesis of crystalline, condensed, graphitic carbon nitride, Chemistry – Eur. J., 14 (2008) 8177–8182.
[32] G. Wu, S. Gan, L. Cui, Y. Xu, Preparation and characterization of PES/TiO_2 composite membranes, Appl. Surf. Sci., 254 (2008) 7080–7086.
[33] Y. Yang, P. Wang, Preparation and characterizations of a new PS/TiO_2 hybrid membranes by sol–gel process, Polymer, 47 (2006) 2683–2688.
[34] S.E. Solovyov, Reactivity of gas barrier membranes filled with reactive particulates, J. Phys. Chem. B, 110 (2006) 17977–17986.